

HierEdit : Region-Aware Hierarchical Diffusion for Efficient High-Resolution Editing

Yuyao Zhang
Dartmouth College

Alexander Huang-Menders
Dartmouth College

Yu-Wing Tai
Dartmouth College



Figure 1. **Demo of HierEdit**. Our method enables efficient, high-fidelity local editing at ultra-high resolution (2K and 4K here) without the need of 4K data for training. We support both instruction editing and both text- and image-guided inpainting. On commodity resolution (1K) we are much faster.

Abstract

High-resolution image editing is essential for professional and creative applications, yet existing multimodal diffusion-based editors remain computationally inefficient and constrained to relatively low resolutions. Current approaches redundantly process the entire image canvas or rely on large-scale high-resolution datasets, resulting in substantial training and inference costs. We introduce **HierEdit**, a region-aware hierarchical diffusion framework designed for efficient and scalable high-resolution image editing. Our method first performs edits on a low-resolution proxy using an off-the-shelf editing model to generate a reference and to localize the modified regions. A hierarchical local-window diffusion model (**Local-Window MMDiT**) that refines only edited regions within the original high-res image, while reusing the unaltered regions as conditioning inputs. The low-resolution proxy further provides structural guidance

and intermediate denoising supervision (**Inference Acceleration**), ensuring consistent global semantics and stable generation without the need for full-resolution attention computation. This targeted and hierarchical design enables fast, high-fidelity editing of images up to 4K resolution without any specialized high-resolution training data. Extensive experiments demonstrate that **HierEdit** achieves competitive visual quality on commodity-resolution datasets while significantly accelerating inference and extending seamlessly to ultra-high-resolution 4K editing. Please check our [Project Page](#).

1. Introduction

Text-guided image editing has become a powerful tool for creative expression and content manipulation, enabling users to modify images with precise semantic control [4, 39, 43]. However, the computational cost of dense atten-

tion [11, 12] scales quadratically with resolution, limiting their use in high-resolution workflows. Most state-of-the-art techniques remain constrained to standard resolutions, typically below $1K \times 1K$, which restricts their applicability in professional domains such as digital advertising, cinematography, and high-fidelity visualization, where ultra-high-resolution (UHR) outputs (4K and above) are essential.

Image editing tasks can be broadly categorized into *global* edits, like applying a new artistic style, which require processing the entire image, and *local* edits, which target specific objects or regions, such as “Remove the rightmost person.” or “Replace an apple with an orange.” Many practical applications fall into the latter category, yet existing models handle them inefficiently. Some re-render the entire image for minor changes, wasting computation on untouched regions, while others rely on inpainting, which ignores interactions with external areas and often produces border artifacts. The key challenge is not just scaling to higher resolutions, but enabling targeted local edits efficiently. Recent hierarchical local attention architectures show promise for efficient *generation* [38], but their use in editing remains largely unexplored.

In this work, we introduce **HierEdit**, a novel framework for efficient, high-resolution local image editing. To avoid costly dense attention across the entire image, we employ **Local-Window MMDiT**, which performs hierarchical local-window attention and surgically targets only regions requiring modification. The pipeline begins by down-sampling the high-resolution input to a standard-resolution proxy (e.g., $1K \rightarrow 256$), where an off-the-shelf editing model [3] generates edits. This low-resolution proxy serves two roles: (1) providing semantic guidance and a refined edit mask to localize modifications accurately, and (2) serving as an intermediate initialization to skip early denoising steps. Guided by the proxy, the Local-Window MMDiT then re-synthesizes only the masked patches in the original high-resolution image, preserving global consistency and pixel fidelity. Finally, **inference acceleration** techniques, including intermediate flow initialization and kernel optimizations, further reduce runtime while enabling ultra-high-resolution editing.

This targeted methodology achieves substantial gains in computational efficiency, memory usage, and inference speed, particularly for common local editing tasks. By restricting expensive dense attention operations to sparse local-window attention on a small subset of the image, **HierEdit** decouples performance from image resolution, enabling rapid, iterative edits that would be impractical with dense-attention models. A direct benefit of this efficiency is high scalability, allowing precise editing of ultra-high-resolution (UHR) images such as 4K. Our framework thus provides a practical and generalizable solution for high-

fidelity local editing.

Our main contributions are summarized as follows:

- We introduce a low-resolution edited proxy to guide high-resolution local editing, providing semantic guidance, a refined edit mask, and an intermediate initialization for skipping early denoising steps, achieving up to $> 6\times$ faster performance in 1K resolution (more gains at higher resolutions) with state-of-the-art quality.
- We propose **Local-Window MMDiT**, a hierarchical diffusion model that replaces dense attention with sparse local-window attention, operating only on regions requiring modification, dramatically improving computational efficiency.
- We incorporate **Inference Acceleration** techniques, including intermediate flow initialization and kernel-level optimizations, further reducing runtime for high-resolution editing.
- Our framework enables fast, high-fidelity editing on ultra-high-resolution (4K) images without requiring 4K training data, making practical UHR editing feasible for professional workflows.

2. Related Work

Controllable Image Generation.

Text-to-image (T2I) generation has advanced rapidly with diffusion models, progressing from pixel-space methods such as GLIDE [37] and Imagen [45] to efficient latent-space frameworks such as Stable Diffusion [43] and Raphael [63]. Improvements in multimodal alignment, e.g., DALLE-2 [41] and Playground [25], and in architecture design, e.g., Diffusion Transformers [38], PixArt [8], and FLUX [3], have further improved image fidelity and diversity. Recent systems [4, 6, 8, 9, 14, 17, 25, 27, 38, 39, 43, 59, 60, 63] adopt cross-attention and diffusion transformer (DiT) architectures to achieve near-photorealistic synthesis at resolutions up to $1K \times 1K$, forming a strong foundation for controllable generation.

Despite this progress, fine-grained spatial and semantic control remains challenging. Personalization methods [16, 44] enable subject-specific generation but typically require instance-level fine-tuning. Structured control methods such as ControlNet [74] and GLIGEN [26] provide spatial conditioning through edge maps or bounding boxes, but rely on detailed external guidance and offer limited holistic scene reasoning. Domain-specialized methods such as Raphael [63] improve fidelity at high computational cost, while lightweight adapters such as Attend [7] reduce overhead but remain limited on complex compositions. Autoregressive frameworks, including LlamaGen [51], Show-O [61], and Janus-Pro [10], support prompt-driven synthesis but often suffer from weaker spatial consistency. Overall, most existing approaches are still constrained by quadratic

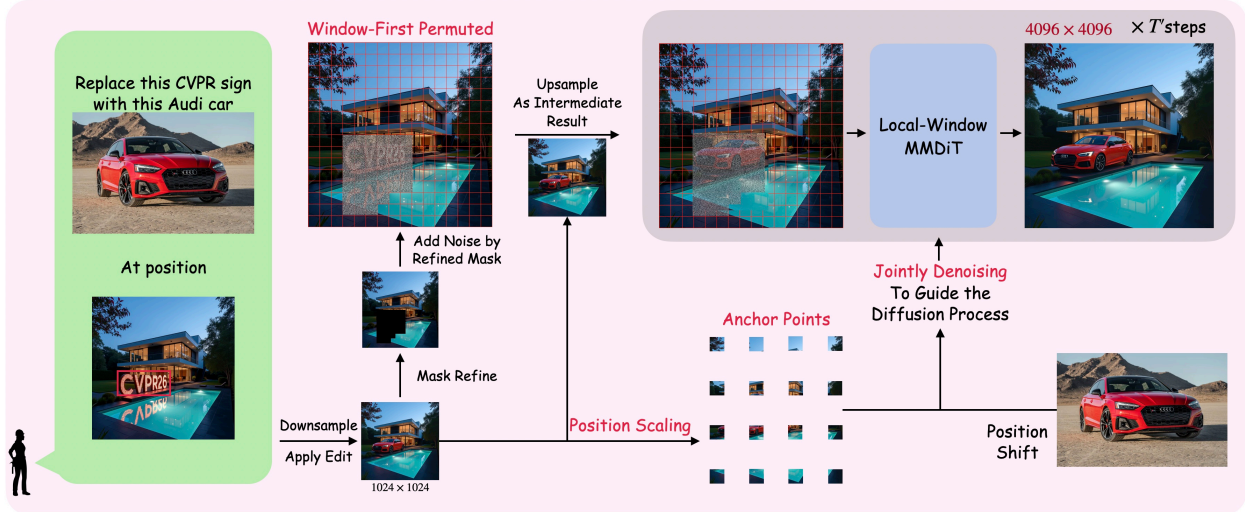


Figure 2. Schematic of the **HierEdit** framework. We employ editing of a downsampled input image and region bounding to identify the edited patches and obtain the low-resolution proxy. We then proceed to input concatenation, re-permutation, and positional encoding. Finally, we pass this input to our hierarchical local-window MMDiT model, which generates the high resolution edited results with less denoising steps as upsampled low-resolution proxy can serve as intermediate denoising result.

attention and limited high-resolution training data, hindering scalable ultra-high-resolution synthesis and region-aware editing.

High-Resolution Image Synthesis. Real-world applications increasingly demand $4K$ or higher resolutions, driving research beyond the $1K \times 1K$ barrier. Works such as PixArt- Σ and SANA 1.5 [60] achieve near- $4K$ synthesis via extensive high-resolution pretraining, while others [20, 29, 42, 55, 58, 66, 70, 79] rely on fine-tuning or training-from-scratch with curated datasets. For instance, [70] employs wavelet supervision to enhance detail clarity, and [66] introduces lightweight fine-tuning for higher-resolution adaptation. Despite their effectiveness, these methods remain limited by the scarcity of high-quality high-resolution data and high GPU requirements. One work [76] demonstrates a promising direction by leveraging scaled RoPE embeddings and window-permuted global-local attention to scale pretrained diffusion models beyond their pretrained resolutions; we build on this idea in the architecture design of our method.

More recent training-free strategies [5, 15, 18, 21, 23, 31, 40, 49, 56] avoid data collection by leveraging pretrained models directly. While promising, these approaches often inherit significant runtime and memory overhead, limiting accessibility for broader use.

Attention Acceleration. As image and video resolutions grow, quadratic attention becomes the main bottleneck. Linear-attention variants like the SANA series [59, 60, 80] reduce complexity but suffer from non-injective mappings and lower attention spikiness [19, 36, 75], often causing local detail inconsistencies. System-level optimizations

such as FlashAttention [11, 12, 46], quantization [69, 71], and sparsity-based methods [13, 28] improve efficiency via hardware-aware acceleration. Architectures like LongFormer [2] and SwinFormer [32] use local windows but still process the full image with static attention. Recent works [24, 57, 62, 64, 67, 68, 72] employ block-sparse or compressed attention in diffusion transformers, achieving moderate speedups (1.5–1.8 \times) at some cost to fine-grained fidelity. Complementary methods like OminiControl2 [52, 53] speed up conditional diffusion by restricting computation to masked regions but still rely on user-provided masks and predefined edit scopes. In contrast, our approach automatically localizes editable regions using low-resolution proxies and applies content-aware sparse attention, enabling efficient ultra-high-resolution editing without manual masks or retraining.

3. Method

Figure 2 presents an overview of the proposed **HierEdit** framework, which leverages low-resolution edits to guide high-resolution image editing efficiently. Given a high-resolution input image, a text prompt, and optional control inputs, we first downsample the image and apply edits using a state-of-the-art (SOTA) image editing model. Comparing the edited low-resolution output with the original image produces a refined mask that accurately localizes the edited regions. These refined regions, together with the low-resolution edits, serve as references for high-resolution, region-aware generation.

In Section 3.1, we review the foundational preliminaries, including rectified flow models and the Multi-Modal Diffusion Transformer (MMDiT) backbone with RoPE position

encoding. Section 3.2 describes low-resolution guided region refinement, where the refined mask and edited low-resolution image are computed to guide subsequent high-resolution editing. Section 3.3 introduces Local-Window MMDiT, which combines efficient local-window attention, joint denoising of integrated token sequences, and low-resolution anchors to maintain global semantic coherence while reducing computation. Finally, Section 3.4 presents inference acceleration technique with intermediate flow initialization to further speed up high-resolution generation.

3.1. Preliminaries

Rectified Flow Models [30]. Flow-based generative models learn a continuous transformation between a data sample X_0 and a simple reference distribution X_1 by integrating an ODE

$$\frac{dZ_t}{dt} = V(Z_t, t),$$

where V is a learned velocity field. Sampling is performed by drawing $Z_1 \sim \mathcal{N}(0, I)$ and solving the ODE backwards to obtain Z_0 . Rectified flows constrain the intermediate states to follow a linear path,

$$Z_t = (1 - t)X_0 + tX_1,$$

which produces straight and stable trajectories that require only a small number of integration steps.

MMDiT with RoPE Position Encoding. The Multi-Modal Diffusion Transformer (MMDiT) is the standard backbone of recent text-to-image models [3, 6, 17]. It processes a text token sequence C_T and a noisy image token sequence X , which are concatenated as $[C_T; X]$ and jointly encoded through a unified Multi-Modal Attention (MMA) layer. Spatial structure in image tokens is represented using Rotary Position Embeddings (RoPE) [50], applying a position-dependent rotation $\text{Rot}(i, j)$ to each spatial token:

$$X_{i,j} = X_{i,j} \cdot \text{Rot}(i, j).$$

The MMA mechanism performs standard self-attention over the combined sequence:

$$\text{MMA}([C_T; X]) = \text{Softmax}\left(\frac{QK^\top}{\sqrt{d}}\right)V,$$

where Q, K, V denote the projection matrices for both text and image tokens. This formulation enables dense bidirectional interaction across modalities. The usage of RoPE enables the model to generate image of sizes within a pre-trained range, regardless of where it is on the latent grid.

3.2. Low-Resolution Guided Region Refinement

Given a high-resolution input image X_{Hr} , a text prompt, and an optional control image $X_{Control}$, we first downsample X_{Hr} to X_{Lr} (e.g., $1K \times 1K \rightarrow 256 \times 256$). We then

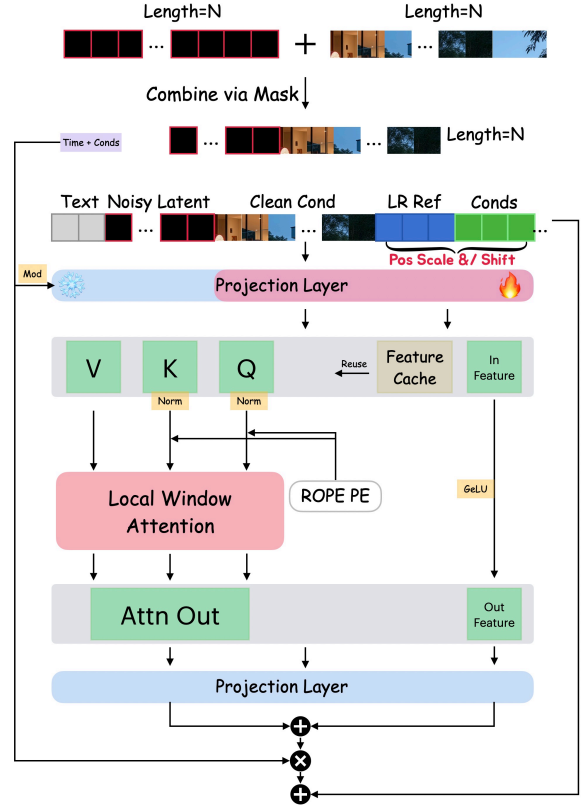


Figure 3. The illustration of jointly denoising the integrated token sequence via Local-Window MMDiT. We prune the tokens from $2N$ to N by the edit mask and only denoise the edited region. All tokens are concatenated together while conditions and low-resolution reference are processed via finetuned layers, and original weights for the image latent. "Fire" and "Snowflake" signs mean LoRA finetuning and frozen weights.

feed X_{Lr} , together with the prompt and optional control input, into a unified image generation and editing model [3] to perform text-guided or multimodal conditional editing, producing an edited low-resolution image X'_{Lr} that guides the subsequent high-resolution editing branch.

Since user-provided masks M are often imperfect for complex effects such as reflections, shadows, and occlusions, we derive a refined mask \tilde{M} by comparing X'_{Lr} with X_{Lr} at the pixel level to better localize the edited regions. Overall, the pipeline downsamples X_{Hr} to X_{Lr} , obtains X'_{Lr} through low-resolution editing, and computes \tilde{M} for precise high-resolution editing. This refined mask ensures better alignment between the final high-resolution edits and the intended semantic and contextual modifications.

3.3. Local-Window MMDiT

Efficient Local Window Attention. DiT-based generative models rely heavily on self-attention, whose quadratic computational cost becomes prohibitive as image size increases. For an image of size $H \times W$ after encoder downsampling,

the number of spatial tokens is $N = H \cdot W$, resulting in $O(N^2)$ complexity. To address this, we partition the high-resolution latent $X \in \mathbb{R}^{H \times W}$ into non-overlapping windows x_i of size l , bounded by the pretrained resolution (e.g., 1024), with $i = \frac{H}{l} \times \frac{W}{l}$ windows in total. Attention is computed only within each window, reducing complexity to $O(\frac{H}{l} \cdot \frac{W}{l} \cdot (l^2)^2) = O(N \cdot l^2)$. For example, scaling from 1024×1024 to 4096×4096 reduces computation by $256 \times$.

In practice, we set $l = 16$, corresponding to 256 pixels in the original image, balancing accuracy and efficiency: smaller windows speed up attention but overly small windows underutilize GPU kernels. Importantly, while this analysis assumes processing all windows, in practice we compute attention only for masked local windows requiring edits. As a result, runtime scales linearly with the number of local windows being processed, further accelerating high-resolution generation. Because each local window has a fixed positional embedding range, the model can reliably generate content within each block, enabling ultra-high-resolution synthesis. To prevent block artifacts introduced by the non-overlapping windows, we allow each window to attend to boundary tokens of adjacent windows, enabling information flow among them without breaking the linearized computational burden.

Jointly Denoising Integrated Token Sequence. In text- or image-guided editing tasks, the model typically processes two input sequences of equal length: the masked source image X_{origin} and its corresponding noisy latent X_{noise} . Naively concatenating these doubles the sequence length and quadruples attention memory cost.

To address this, we construct a unified token sequence by assigning each spatial location a single role. Unmasked regions from X_{origin} , denoted $C^{\text{mask}=0}$, serve as *condition tokens* that provide static contextual information and are not denoised, while masked regions from $X_{\text{noise}}^{\text{mask}=1}$ are *noisy tokens* that undergo iterative denoising. Combining these into a single sequence $X_{\text{integrated}} = [C^{\text{mask}=0}; X_{\text{noise}}^{\text{mask}=1}]$ reduces the total length to that of a single image, preserving computational efficiency. Because condition tokens remain fixed across diffusion steps, their Key and Value projections can be cached and reused after one single forward pass (Feature Caching), significantly accelerating inference. To prevent noise contamination, condition tokens attend only to other condition tokens and not to the noisy tokens or text tokens. To better preserve the details in the condition images, our framework incorporates additional guidance signals by concatenating them as extra tokens along the sequence dimension. All conditions interact with the generation tokens through the self-attention layers of the pretrained DiT, allowing us to leverage the original model weights without architectural modification; only lightweight LoRA modules are fine-tuned to adapt the model to the new conditioning

scheme. Figure 3 illustrates the overall architecture. Speed improvements are demonstrated in the ablation study.

Maintaining Global Semantics via Low-Res Anchors.

Partitioning a high-resolution image into independent local windows can introduce discontinuities and disrupt global semantic coherence. We observe that long-range dependencies primarily govern global structure and spatial layout, while fine-grained details depend on local interactions. To preserve global consistency, we leverage a pre-edited low-resolution image $X'_{Lr} \in \mathbb{R}^{h \times w}$, which encapsulates holistic contextual information. Pixel positions in this image are indexed as (m, n) with $m \in 0, \dots, h-1$ and $n \in 0, \dots, w-1$.

We define a scaling ratio $\rho = \frac{H}{h}$ (empirically set to 4) and map low-resolution coordinates to high-resolution space as $(\tilde{m}, \tilde{n}) = (\rho \cdot m, \rho \cdot n)$. Each projected token $X'_{Lr}[\tilde{m}, \tilde{n}]$ provides contextual cues for the corresponding high-resolution region. Reference image tokens are similarly scaled and shifted, $(m', n') = \rho' \cdot ((m', n') + \Delta)$, where ρ' is the size ratio and Δ the position offset.

We then construct a unified token sequence $[C_T, X_{\text{integrated}}, X'_{Lr}, X_{\text{control}}, \dots]$ and process all conditions with the standard DiT encoders the base model use. After scaling and shifting position embeddings, LoRA only adapts the attention projection layers to the new features. To prevent noisy latents from affecting conditions, only self-attention is applied to the condition tokens.

Training uses a standard flow-matching loss, which aims at teaching model about the new attention pattern. This design provides three key benefits: (1) training efficiency by updating only a compact set of LoRA parameters; (2) adaptation using commodity-resolution data (1K resolution); and (3) seamless extension to ultra-high-resolution generation (e.g., 4K) since local-window attention focuses on pretrained-size regions, making it resolution-invariant.

3.4. Inference Acceleration

Intermediate Flow Initialization. As we already have the low-resolution reference, which has the same structure as the high resolution results, the only difference is the high frequency details. Therefore we first resize the low-resolution reference to the same size as the target image, sharpen it, and scale noise to the intermediate timestep t to obtain X_{ref}^t . For a given flow, the sampling of high-resolution generation starts from the noisy variant of X_{ref}^t , which can be expressed as:

$$X_{\text{hr}}^t = \alpha X_{\text{hr}}^1 + (1 - \alpha) X_{\text{ref}}^t,$$

where X_{hr}^t is the initialization of the high-resolution sampling, X_{hr}^1 is Gaussian noise, and $\alpha \in (0, 1)$ is the noise addition ratio. Such initialization allows skipping the early stage in high-resolution generation by providing the low-frequency components. Thus we facilitate faster inference

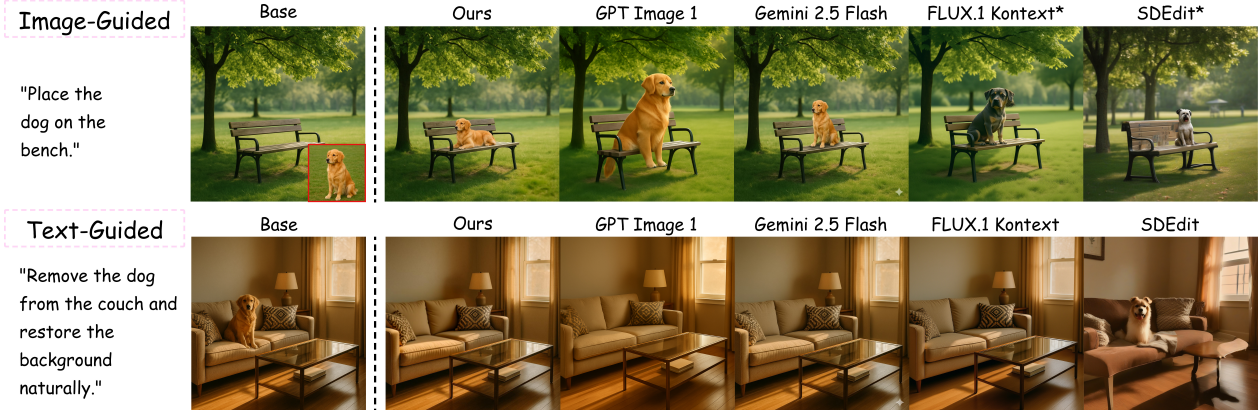


Figure 4. Qualitative comparison for instructional editing. The asterisk * indicates that the model does not take a control image. We demonstrate more accurate subject integration by not only preserving subject identity, but also integrating it more naturally with the scene context. We also match the best lighting preservation.

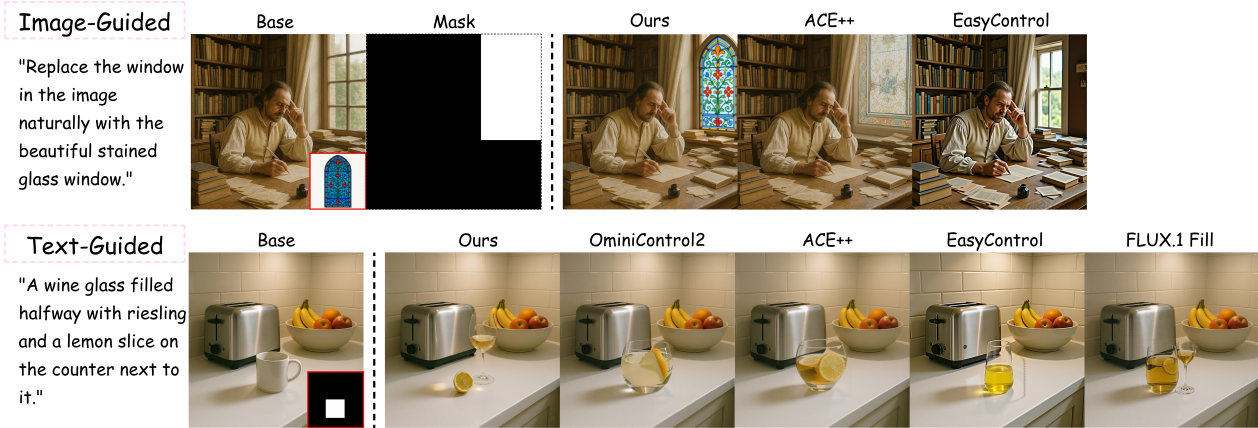


Figure 5. Qualitative comparison of inpainting-based editing methods. The proposed HierEdit demonstrates better performance in preserving unmodified regions while maintaining natural integration of edited content.

by reducing redundant denoising steps from T to T' , empirically $T = 28$ and $T' = 10$.

4. Experiments

4.1. Comparison with State-of-the-Art Methods

We compare **HierEdit** with baselines from two different categories of editing, (1) instructional editing and (2) inpainting based editing. Instructional editing methods includes GPT Image 1 [1], Gemini 2.5 Flash Image [54], FLUX.1 Kontext [4] and SDEdit [35]. For inpainting based editing we compare our method with FLUX-Fill [3], OmniControl2 [53], ACE++ [34], EasyControl [78].¹

Qualitative Results and Comparisons. Figure 1 showcases **HierEdit**'s performance on diverse editing tasks at ultra-high resolutions (2K and 4K), demonstrating high visual fidelity and significant speed advantages over prior methods. Figure 4 presents comparisons on instruction-

based edits using text-only or text-image prompts. In the first row, guided by both text and image, GPT Image 1 produces an object at the wrong scale, while FLUX.1 Kontext and SDEdit fail to generate the correct object, with SDEdit also introducing background distortions. In the second row for text-only edits, GPT Image 1 and FLUX Kontext fail to preserve the couch lighting, and Gemini and SDEdit significantly alter the global scene.

Figure 5 shows inpainting-based editing. In the first row, EasyControl fails to place the control image correctly, and ACE++ adds a window with incorrect color and pattern. We did not compare with OmniControl2 as their checkpoints are unavailable for subject-driven inpainting. In the second row, FLUX.1 Fill generates two glasses instead of one, EasyControl produces off-colored wine with shadow artifacts, and OmniControl2 and ACE++ place the lemon incorrectly inside the glass rather than beside it.

Quantitative Comparison. Table 1 reports quantitative results for instruction-based editing, where **HierEdit** achieves competitive performance across all benchmarks. Table 2 summarizes mask-guided and inpainting-based

¹See supplementary materials for evaluation metrics, benchmarks, and implementation details.

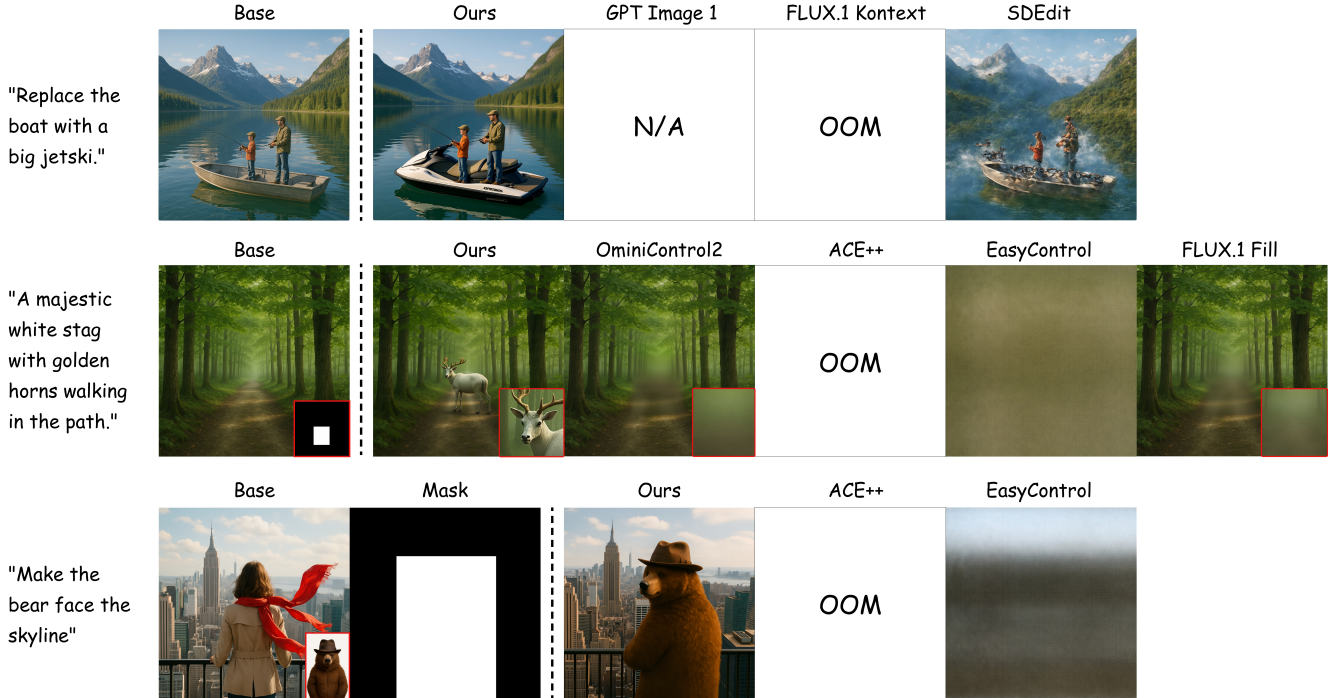


Figure 6. Comparison at 4K resolution for text guided editing, text-guided inpainting, and subject-guided inpainting. GPT-Image-1 was incapable of generating resolutions higher than 1K by design and ACE++ was unable to run 4K inference with 96GB of GPU memory. Our method succeeded in generating the results while the rest of others failed.

Task	Method	CompBench		EmuEdit		ImgEdit	I2EBench
		CLIP \uparrow	SSIM \uparrow	CLIP $_{dir}$ \uparrow	DINO \uparrow	Composite \uparrow	SSIM \uparrow
Text-guided editing	SDEdit	18.5	0.351	0.053	0.159	1.46	0.355
	FLUX.1 Kontext	20.8	0.954	0.116	0.840	3.45	<u>0.501</u>
	GPT-Image-1	18.9	0.191	0.132	0.697	4.45	0.478
	Ours	<u>20.6</u>	<u>0.949</u>	<u>0.117</u>	<u>0.833</u>	<u>3.51</u>	0.508

Table 1. Quantitative comparison of text guided image editing methods across CompBench, EmuEdit, ImgEdit, and I2EBench benchmarks.

editing, showing that our approach consistently matches or outperforms baselines while offering substantial efficiency gains. Table 3 presents average inference times for inpainting at different resolutions and edit ratios. **HierEdit** is the fastest across all configurations, with OminiControl2 consistently second. Notably, other methods often produce noisy or malformed outputs at high resolutions, making them inadequate for realistic edits. We provide full high-resolution stress tests in the supplementals, demonstrating that **HierEdit** is the only model capable of high-quality editing at these scales.

5. High-Resolution Comparison

We compare our high-resolution generation results with those of other models, which fail to produce meaningful outputs. As shown in Figure 6, our method successfully generates high-quality 4K images, whereas the baselines either produce no content within the mask or fail entirely due

to out-of-memory errors.

Efficiency Comparison. Table 3 compares inference speed across methods. At 1K resolution, our approach is up to 6.0 \times faster than competing models, with even larger margins at higher resolutions. When varying the proportion of the edited region, our method remains highly efficient because computation is restricted to the modified areas, whereas competing approaches exhibit nearly constant runtime regardless of edit extent.

6. Ablation Study

We conduct a series of ablation experiments to evaluate the contribution of key components in our pipeline, the need for the bounding box refinement, and the effect of step reduction during inference (see supplementary materials).

Impact of Acceleration Components. Table 4 reports the effect of removing different acceleration modules. *LWA* de-

Task	Method	FID↓	PSNR↑	CLIP-T↑	CLIP-I↑	Latency↓	Time/iter↓
Text-guided inpainting	FLUX-Fill	56.1	<u>19.23</u>	0.338	0.923	21.4s	0.42s
	OminiControl2*	39.2	19.11	0.339	0.921	<u>8.25s</u>	<u>0.29s</u>
	ACE++	37.2	18.81	0.342	0.929	22.5s	0.80s
	EasyControl	108.6	15.38	0.331	0.887	14.5s	0.55s
	Ours	<u>39.5</u>	19.31	<u>0.340</u>	<u>0.926</u>	6.97s	0.24s
Image-guided inpainting	ACE++	<u>42.5</u>	16.21	<u>0.346</u>	0.959	52.9s	1.9s
	EasyControl	108.3	14.89	0.342	0.932	<u>17.3s</u>	<u>0.65s</u>
	Ours	41.9	<u>15.82</u>	0.349	<u>0.939</u>	7.84s	0.26s

Table 2. Quantitative comparison of text-guided and image-guided FLUX-based inpainting methods across fidelity, perceptual, and efficiency metrics on $1K \times 1K$ resolution.

Edit %	Method	1K	2K	3K	4K
25%	OminiControl2	<u>5.98s</u>	<u>21.5s</u>	<u>63.3s</u>	<u>155s</u>
	FLUX-Fill	21.4s	113s	383s	1064s
	ACE++	25.1s	424s	—	—
	EasyControl	27.5s	69.2s	222s	590s
	Ours	4.51s	15.6s	35.6s	91.4s
50%	OminiControl2	<u>8.47s</u>	<u>35.8s</u>	<u>113s</u>	<u>286s</u>
	FLUX-Fill	21.5s	113s	383s	1065s
	ACE++	25.0s	425s	—	—
	EasyControl	29.0s	69.3s	224s	597s
	Ours	6.74s	19.2s	55.7s	173s
75%	OminiControl2	<u>11.0s</u>	<u>53.8s</u>	<u>164s</u>	<u>408s</u>
	FLUX-Fill	21.2s	112s	383s	1052s
	ACE++	25.0s	426s	—	—
	EasyControl	29.2s	69.4s	221s	587s
	Ours	8.32s	23.0s	84.1s	227s

Table 3. Speed comparison of different methods across varying edit ratios and resolutions. Results marked by “—” were unable to run on 96GB of GPU memory with expandable segments.

Method	Speed↓	PSNR↑	CLIP-T↑	CLIP-I↑
Ours	2.34	<u>19.01</u>	0.339	0.931
-LWA	4.98 ($\times 2.13$)	18.84	0.336	0.922
-LWA-FC	9.32 ($\times 3.98$)	18.96	<u>0.338</u>	<u>0.923</u>
-LWA-FC-TI	29.12 ($\times 12.4$)	19.03	0.339	<u>0.923</u>

Table 4. Ablation of speed (without low-res denoising part) difference on design components of our method on $1K \times 1K$ resolution with 50% edited region. LWA denotes local window attention with Flash Sparse Attention Kernel. The number in the () means how much slower comparing to the full pipeline.

notes the local window attention implemented with a Flash Sparse Attention kernel; *TI* refers to the joint integration of conditional and noisy image tokens (as illustrated in the upper portion of Figure 3); and *FC* represents feature caching, which avoids redundant projections for unchanged regions. We evaluate four configurations: the full model, the model without LWA, without both LWA and FC, and

without LWA, TI, and FC. Experiments are conducted at 1K resolution with 50% of the image edited. The results show that the complete system delivers the best trade-off between speed and fidelity, while progressive removal of components leads to notable degradation in both aspects.

The Need for Bounding Box Refinement. Figure 7 demonstrates the importance of bounding box refinement. In models like EasyControl, the direct usage of the given bounding box causes incorrect shadowing while ours solve this problem.



Figure 7. The inappropriate bounding box will lead to issues in correct shadowing or other artifacts, therefore we need to refine the bounding box.

7. Conclusion

We presented **HierEdit**, a region-aware hierarchical diffusion framework for efficient high-resolution image editing, without requiring ultra-high-resolution training data. Our approach leverages low-resolution proxy guidance, local-window MMDiT, and inference acceleration to process only modified regions with sparse local-window attention, achieving substantial speedups over state-of-the-art methods while preserving visual fidelity. By decoupling computational cost from image resolution, **HierEdit** enables 4K editing that was previously impractical without dense attention or costly high-resolution data. These results demonstrate that combining multi-scale guidance, sparse attention, and targeted acceleration provides a practical and scalable solution for professional workflows demanding ultra-high-resolution outputs.

References

- [1] Josh Achiam, Steven Adler, Sandhini Agarwal, Lama Ahmad, Ilge Akkaya, Florencia Leoni Aleman, Diogo Almeida, Janko Altenschmidt, Sam Altman, Shyamal Anadkat, et al. Gpt-4 technical report. *arXiv preprint arXiv:2303.08774*, 2023. 6
- [2] Iz Beltagy, Matthew E Peters, and Arman Cohan. Longformer: The long-document transformer. *arXiv preprint arXiv:2004.05150*, 2020. 3
- [3] Black Forest Labs. Flux. Black Forest Labs GitHub repository, 2024. Model release. 2, 4, 6, 1
- [4] Black Forest Labs. Flux.1 kontext: Flow matching for in-context image generation and editing in latent space. *arXiv preprint arXiv:2506.15742*, 2025. 1, 2, 6
- [5] Jiazi Bu, Pengyang Ling, Yujie Zhou, Pan Zhang, Tong Wu, Xiaoyi Dong, Yuhang Zang, Yuhang Cao, Dahua Lin, and Jiaqi Wang. Hiflow: Training-free high-resolution image generation with flow-aligned guidance. In *Advances in Neural Information Processing Systems (NeurIPS)*, 2025. 3
- [6] Qi Cai, Yehao Li, Yingwei Pan, Ting Yao, and Tao Mei. Hidream-i1: An open-source high-efficient image generative foundation model. In *ACM International Conference on Multimedia (ACM MM)*, page 13636–13639, New York, NY, USA, 2025. Association for Computing Machinery. 2, 4
- [7] Hila Chefer, Yuval Alaluf, Yael Vinker, Lior Wolf, and Daniel Cohen-Or. Attend-and-excite: Attention-based semantic guidance for text-to-image diffusion models. *ACM Transactions on Graphics (TOG)*, 42(4):1–10, 2023. 2
- [8] Junsong Chen, Yue Wu, Simian Luo, Enze Xie, Sayak Paul, Ping Luo, Hang Zhao, and Zhenguo Li. Pixart- δ : Fast and controllable image generation with latent consistency models. *arXiv preprint arXiv:2401.05252*, 2024. 2
- [9] Junsong Chen, Jincheng YU, Chongjian GE, Lewei Yao, Enze Xie, Zhongdao Wang, James Kwok, Ping Luo, Huchuan Lu, and Zhenguo Li. Pixart- α : Fast training of diffusion transformer for photorealistic text-to-image synthesis. In *International Conference on Learning Representations (ICLR)*, 2024. 2
- [10] Xiaokang Chen, Zhiyu Wu, Xingchao Liu, Zizheng Pan, Wen Liu, Zhenda Xie, Xingkai Yu, and Chong Ruan. Januspro: Unified multimodal understanding and generation with data and model scaling. *arXiv preprint arXiv:2501.17811*, 2025. 2
- [11] Tri Dao. Flashattention-2: Faster attention with better parallelism and work partitioning. In *International Conference on Learning Representations (ICLR)*, 2024. 2, 3
- [12] Tri Dao, Daniel Y. Fu, Stefano Ermon, Atri Rudra, and Christopher Ré. Flashattention: Fast and memory-efficient exact attention with io-awareness. In *Advances in Neural Information Processing Systems (NeurIPS)*, pages 16344–16359, 2022. 2, 3
- [13] Yichuan Deng, Zhao Song, Jing Xiong, and Chiwan Yang. How sparse attention approximates exact attention? your attention is naturally n^c -sparse. *arXiv preprint arXiv:2404.02690*, 2025. 3
- [14] Ming Ding, Zhuoyi Yang, Wenyi Hong, Wendi Zheng, Chang Zhou, Da Yin, Junyang Lin, Xu Zou, Zhou Shao, Hongxia Yang, and Jie Tang. Cogview: mastering text-to-image generation via transformers. In *Conference on Neural Information Processing Systems (NeurIPS)*, Red Hook, NY, USA, 2021. Curran Associates Inc. 2
- [15] Ruoyi Du, Dongyang Liu, Le Zhuo, Qin Qi, Hongsheng Li, Zhanyu Ma, and Peng Gao. I-max: Maximize the resolution potential of pre-trained rectified flow transformers with projected flow. *arXiv preprint arXiv:2410.07536*, 2024. 3
- [16] Rinon Gal, Yuval Alaluf, Yuval Atzmon, Or Patashnik, Amit H Bermano, Gal Chechik, and Daniel Cohen-Or. An image is worth one word: Personalizing text-to-image generation using textual inversion. In *International Conference on Learning Representations (ICLR)*, 2023. 2
- [17] Yu Gao, Lixue Gong, Qiushan Guo, Xiaoxia Hou, Zhichao Lai, Fanshi Li, Liang Li, Xiaochen Lian, Chao Liao, Liyang Liu, et al. Seedream 3.0 technical report. *arXiv preprint arXiv:2504.11346*, 2025. 2, 4
- [18] Lanqing Guo, Yingqing He, Haoxin Chen, Menghan Xia, Xiaodong Cun, Yufei Wang, Siyu Huang, Yong Zhang, Xintao Wang, Qifeng Chen, et al. Make a cheap scaling: A self-cascade diffusion model for higher-resolution adaptation. In *European Conference on Computer Vision (ECCV)*, pages 39–55. Springer, 2024. 3
- [19] Dongchen Han, Yifan Pu, Zhuofan Xia, Yizeng Han, Xuran Pan, Xiu Li, Jiwen Lu, Shiji Song, and Gao Huang. Bridging the divide: Reconsidering softmax and linear attention. In *Advances in Neural Information Processing Systems (NeurIPS)*, pages 79221–79245, 2024. 3
- [20] Emiel Hoogeboom, Jonathan Heek, and Tim Salimans. simple diffusion: End-to-end diffusion for high resolution images. In *International Conference on Machine Learning (ICML)*, pages 13213–13232. PMLR, 2023. 3
- [21] Linjiang Huang, Rongyao Fang, Aiping Zhang, Guanglu Song, Si Liu, Yu Liu, and Hongsheng Li. Fouriscale: A frequency perspective on training-free high-resolution image synthesis. In *European Conference on Computer Vision (ECCV)*, pages 196–212. Springer, 2024. 3
- [22] Bohan Jia, Wenxuan Huang, Yuntian Tang, Junbo Qiao, Jincheng Liao, Shaosheng Cao, Fei Zhao, Zhaopeng Feng, Zhouhong Gu, Zhenfei Yin, Lei Bai, Wanli Ouyang, Lin Chen, Fei Zhao, Zihan Wang, Yuan Xie, and Shaohui Lin. Compbench: Benchmarking complex instruction-guided image editing. *arXiv preprint arXiv:2505.12200*, 2025. 1
- [23] Younhyun Kim, Geunmin Hwang, Junyu Zhang, and Eunbyung Park. Diffusehigh: Training-free progressive high-resolution image synthesis through structure guidance. In *Proceedings of the AAAI Conference on Artificial Intelligence*, pages 4338–4346, 2025. 3
- [24] Xunhao Lai, Jianqiao Lu, Yao Luo, Yiyuan Ma, and Xun Zhou. Flexprefill: A context-aware sparse attention mechanism for efficient long-sequence inference. In *International Conference on Learning Representations (ICLR)*, 2025. 3
- [25] Daiqing Li, Aleks Kamko, Ehsan Akhgari, Ali Sabet, Linmiao Xu, and Suhail Doshi. Playground v2. 5: Three insights towards enhancing aesthetic quality in text-to-image generation. *arXiv preprint arXiv:2402.17245*, 2024. 2
- [26] Yuheng Li, Haotian Liu, Qingyang Wu, Fangzhou Mu, Jianwei Yang, Jianfeng Gao, Chunyuan Li, and Yong Jae Lee.

- Gligen: Open-set grounded text-to-image generation. In *Proceedings of the IEEE/CVF Conference on Computer Vision and Pattern Recognition*, pages 22511–22521, 2023. 2
- [27] Zhimin Li, Jianwei Zhang, Qin Lin, Jiangfeng Xiong, Yanxin Long, Xincheng Deng, Yingfang Zhang, Xingchao Liu, Minbin Huang, Zedong Xiao, et al. Hunyuan-dit: A powerful multi-resolution diffusion transformer with fine-grained chinese understanding. *arXiv preprint arXiv:2405.08748*, 2024. 2
- [28] Liu Liu, Zheng Qu, Zhaodong Chen, Fengbin Tu, Yufei Ding, and Yuan Xie. Dynamic sparse attention for scalable transformer acceleration. *IEEE Transactions on Computers (TC)*, 71(12):3165–3178, 2022. 3
- [29] Songhua Liu, Weihao Yu, Zhenxiong Tan, and Xinchao Wang. Linfusion: 1 gpu, 1 minute, 16k image. *arXiv preprint arXiv:2409.02097*, 2024. 3
- [30] Xingchao Liu, Chengyue Gong, and Qiang Liu. Flow straight and fast: Learning to generate and transfer data with rectified flow. In *International Conference on Learning Representations (ICLR)*, 2023. 4
- [31] Xinyu Liu, Yingqing He, Lanqing Guo, Xiang Li, Bu Jin, Peng Li, Yan Li, Chi-Min Chan, Qifeng Chen, Wei Xue, et al. Hiprompt: Tuning-free higher-resolution generation with hierarchical mllm prompts. *arXiv preprint arXiv:2409.02919*, 2024. 3
- [32] Ze Liu, Yutong Lin, Yue Cao, Han Hu, Yixuan Wei, Zheng Zhang, Stephen Lin, and Baining Guo. Swin transformer: Hierarchical vision transformer using shifted windows. In *Proceedings of the IEEE/CVF International Conference on Computer Vision*, pages 10012–10022, 2021. 3
- [33] Yiwei Ma, Jiayi Ji, Ke Ye, Weihuang Lin, Zhibin Wang, Yonghan Zheng, Qiang Zhou, Xiaoshuai Sun, and Rongrong Ji. I2ebench: A comprehensive benchmark for instruction-based image editing. In *Advances in Neural Information Processing Systems (NeurIPS)*, pages 41494–41516. Curran Associates, Inc., 2024. 1
- [34] Chaojie Mao, Jingfeng Zhang, Yulin Pan, Zeyinzi Jiang, Zhen Han, Yu Liu, and Jingren Zhou. Ace++: Instruction-based image creation and editing via context-aware content filling. *arXiv preprint arXiv:2501.02487*, 2025. 6
- [35] Chenlin Meng, Yutong He, Yang Song, Jiaming Song, Jiajun Wu, Jun-Yan Zhu, and Stefano Ermon. SDEdit: Guided image synthesis and editing with stochastic differential equations. In *International Conference on Learning Representations (ICLR)*, 2022. 6
- [36] Weikang Meng, Yadan Luo, Xin Li, Dongmei Jiang, and Zheng Zhang. Polaformer: Polarity-aware linear attention for vision transformers. In *International Conference on Learning Representations (ICLR)*, 2025. 3
- [37] Alexander Quinn Nichol, Prafulla Dhariwal, Aditya Ramesh, Pranav Shyam, Pamela Mishkin, Bob McGrew, Ilya Sutskever, and Mark Chen. Glide: Towards photorealistic image generation and editing with text-guided diffusion models. In *International Conference on Machine Learning (ICML)*, pages 16784–16804. PMLR, 2022. 2
- [38] William Peebles and Saining Xie. Scalable diffusion models with transformers. In *Proceedings of the IEEE/CVF International Conference on Computer Vision*, pages 4195–4205, 2023. 2
- [39] Dustin Podell, Zion English, Kyle Lacey, Andreas Blattmann, Tim Dockhorn, Jonas Müller, Joe Penna, and Robin Rombach. Sdxl: Improving latent diffusion models for high-resolution image synthesis. In *International Conference on Learning Representations (ICLR)*, pages 1862–1874, 2024. 1, 2
- [40] Haonan Qiu, Shiwei Zhang, Yujie Wei, Ruihang Chu, Hangjie Yuan, Xiang Wang, Yingya Zhang, and Ziwei Liu. Freescale: Unleashing the resolution of diffusion models via tuning-free scale fusion. In *Proceedings of the IEEE/CVF International Conference on Computer Vision*, pages 16893–16903, 2025. 3
- [41] Aditya Ramesh, Prafulla Dhariwal, Alex Nichol, Casey Chu, and Mark Chen. Hierarchical text-conditional image generation with clip latents. *arXiv preprint arXiv:2204.06125*, 1 (2):3, 2022. 2
- [42] Jingjing Ren, Wenbo Li, Haoyu Chen, Renjing Pei, Bin Shao, Yong Guo, Long Peng, Fenglong Song, and Lei Zhu. Ultrapixel: Advancing ultra high-resolution image synthesis to new peaks. In *Advances in Neural Information Processing Systems (NeurIPS)*, pages 111131–111171. Curran Associates, Inc., 2024. 3
- [43] Robin Rombach, Andreas Blattmann, Dominik Lorenz, Patrick Esser, and Björn Ommer. High-resolution image synthesis with latent diffusion models. In *Proceedings of the IEEE/CVF Conference on Computer Vision and Pattern Recognition*, pages 10684–10695, 2022. 1, 2
- [44] Nataniel Ruiz, Yuanzhen Li, Varun Jampani, Yael Pritch, Michael Rubinstein, and Kfir Aberman. Dreambooth: Fine tuning text-to-image diffusion models for subject-driven generation. In *Proceedings of the IEEE/CVF Conference on Computer Vision and Pattern Recognition*, pages 22500–22510, 2023. 2
- [45] Chitwan Saharia, William Chan, Saurabh Saxena, Lala Li, Jay Whang, Emily L Denton, Kamyar Ghasemipour, Raphael Gontijo Lopes, Burcu Karagol Ayan, Tim Salimans, et al. Photorealistic text-to-image diffusion models with deep language understanding. *Advances in Neural Information Processing Systems (NeurIPS)*, 35:36479–36494, 2022. 2
- [46] Jay Shah, Ganesh Bikshandi, Ying Zhang, Vijay Thakkar, Pradeep Ramani, and Tri Dao. Flashattention-3: Fast and accurate attention with asynchrony and low-precision. In *Advances in Neural Information Processing Systems (NeurIPS)*, pages 68658–68685, 2024. 3
- [47] Shelly Sheynin, Adam Polyak, Uriel Singer, Yuval Kirstain, Amit Zohar, Oron Ashual, Devi Parikh, and Yaniv Taigman. Emu edit: Precise image editing via recognition and generation tasks. In *Proceedings of the IEEE/CVF Conference on Computer Vision and Pattern Recognition*, pages 8871–8879, 2024. 1
- [48] Jingze Shi, Yifan Wu, Bingheng Wu, Yiran Peng, Liangdong Wang, Guang Liu, and Yuyu Luo. Trainable dynamic mask sparse attention. *arXiv preprint arXiv:2508.02124*, 2025. 1
- [49] Shuwei Shi, Wenbo Li, Yuechen Zhang, Jingwen He, Biao Gong, and Yinqiang Zheng. Resmaster: Mastering high-resolution image generation via structural and fine-grained

- guidance. In *Proceedings of the AAAI Conference on Artificial Intelligence*, pages 6887–6895, 2025. 3
- [50] Jianlin Su, Murtadha Ahmed, Yu Lu, Shengfeng Pan, Wen Bo, and Yunfeng Liu. Roformer: Enhanced transformer with rotary position embedding. *Neurocomputing*, 568:127063, 2024. 4
- [51] Peize Sun, Yi Jiang, Shoufa Chen, Shilong Zhang, Bingyue Peng, Ping Luo, and Zehuan Yuan. Autoregressive model beats diffusion: Llama for scalable image generation. *arXiv preprint arXiv:2406.06525*, 2024. 2
- [52] Zhenxiong Tan, Songhua Liu, Xingyi Yang, Qiaochu Xue, and Xinchao Wang. Ominicontrol: Minimal and universal control for diffusion transformer. In *Proceedings of the IEEE/CVF International Conference on Computer Vision*, pages 14940–14950, 2025. 3
- [53] Zhenxiong Tan, Qiaochu Xue, Xingyi Yang, Songhua Liu, and Xinchao Wang. Ominicontrol2: Efficient conditioning for diffusion transformers. *arXiv preprint arXiv:2503.08280*, 2025. 3, 6
- [54] Gemini Team, Rohan Anil, Sebastian Borgeaud, Jean-Baptiste Alayrac, Jiahui Yu, Radu Soricut, Johan Schalkwyk, Andrew M Dai, Anja Hauth, Katie Millican, et al. Gemini: a family of highly capable multimodal models. *arXiv preprint arXiv:2312.11805*, 2023. 6
- [55] Jiayan Teng, Wendi Zheng, Ming Ding, Wenyi Hong, Jianqiao Wangni, Zhuoyi Yang, and Jie Tang. Relay diffusion: Unifying diffusion process across resolutions for image synthesis. In *International Conference on Learning Representations (ICLR)*, 2024. 3
- [56] Haoning Wu, Shaocheng Shen, Qiang Hu, Xiaoyun Zhang, Ya Zhang, and Yanfeng Wang. Megafusion: Extend diffusion models towards higher-resolution image generation without further tuning. In *Proceedings of the IEEE/CVF Winter Conference on Applications of Computer Vision*, pages 3944–3953. IEEE, 2025. 3
- [57] Haocheng Xi, Shuo Yang, Yilong Zhao, Chenfeng Xu, Muyang Li, Xiuyu Li, Yujun Lin, Han Cai, Jintao Zhang, Dacheng Li, et al. Sparse videogen: Accelerating video diffusion transformers with spatial-temporal sparsity. In *International Conference on Machine Learning (ICML)*, pages 68208–68224, 2025. 3
- [58] Enze Xie, Lewei Yao, Han Shi, Zhili Liu, Daquan Zhou, Zhaoqiang Liu, Jiawei Li, and Zhenguo Li. Diffit: Unlocking transferability of large diffusion models via simple parameter-efficient fine-tuning. In *Proceedings of the IEEE/CVF International Conference on Computer Vision*, pages 4230–4239, 2023. 3
- [59] Enze Xie, Junsong Chen, Junyu Chen, Han Cai, Haotian Tang, Yujun Lin, Zhekai Zhang, Muyang Li, Ligeng Zhu, Yao Lu, and Song Han. SANA: Efficient high-resolution text-to-image synthesis with linear diffusion transformers. In *International Conference on Learning Representations (ICLR)*, 2025. 2, 3
- [60] Enze Xie, Junsong Chen, Yuyang Zhao, Jincheng YU, Ligeng Zhu, Yujun Lin, Zhekai Zhang, Muyang Li, Junyu Chen, Han Cai, Bingchen Liu, Daquan Zhou, and Song Han. SANA 1.5: Efficient scaling of training-time and inference-time compute in linear diffusion transformer. In *International Conference on Machine Learning (ICML)*, 2025. 2, 3
- [61] Jinheng Xie, Weijia Mao, Zechen Bai, David Junhao Zhang, Weihao Wang, Kevin Qinghong Lin, Yuchao Gu, Zhijie Chen, Zhenheng Yang, and Mike Zheng Shou. Show-o: One single transformer to unify multimodal understanding and generation. In *International Conference on Learning Representations (ICLR)*, 2025. 2
- [62] Ruyi Xu, Guangxuan Xiao, Haofeng Huang, Junxian Guo, and Song Han. Xattention: Block sparse attention with anti-diagonal scoring. In *International Conference on Machine Learning (ICML)*, pages 69819–69831, 2025. 3
- [63] Zeyue Xue, Guanglu Song, Qiushan Guo, Boxiao Liu, Zhuofan Zong, Yu Liu, and Ping Luo. Raphael: text-to-image generation via large mixture of diffusion paths. In *Conference on Neural Information Processing Systems (NeurIPS)*, Red Hook, NY, USA, 2023. Curran Associates Inc. 2
- [64] Shuo Yang, Haocheng Xi, Yilong Zhao, Muyang Li, Jintao Zhang, Han Cai, Yujun Lin, Xiuyu Li, Chenfeng Xu, Kelly Peng, et al. Sparse videogen2: Accelerate video generation with sparse attention via semantic-aware permutation. In *Advances in Neural Information Processing Systems (NeurIPS)*, 2025. 3
- [65] Yang Ye, Xianyi He, Zongjian Li, Bin Lin, Shenghai Yuan, Zhiyuan Yan, Bohan Hou, and Li Yuan. Imgedit: A unified image editing dataset and benchmark. In *Neural Information Processing Systems Datasets and Benchmarks Track (NeurIPS D&B)*, 2025. 1
- [66] Ruonan Yu, Songhua Liu, Zhenxiong Tan, and Xinchao Wang. Ultra-resolution adaptation with ease. In *International Conference on Machine Learning (ICML)*, 2025. 3
- [67] Zhihang Yuan, Hanling Zhang, Lu Pu, Xuefei Ning, Linfeng Zhang, Tianchen Zhao, Shengen Yan, Guohao Dai, and Yu Wang. Ditfastattn: Attention compression for diffusion transformer models. In *Advances in Neural Information Processing Systems (NeurIPS)*, pages 1196–1219, 2024. 3
- [68] Hanling Zhang, Rundong Su, Zhihang Yuan, Pengtao Chen, Mingzhu Shen, Yibo Fan, Shengen Yan, Guohao Dai, and Yu Wang. Ditfastattnv2: Head-wise attention compression for multi-modality diffusion transformers. In *Proceedings of the IEEE/CVF International Conference on Computer Vision*, pages 16399–16409, 2025. 3
- [69] Jintao Zhang, Haofeng Huang, Pengle Zhang, Jia Wei, Jun Zhu, and Jianfei Chen. Sageattention2: Efficient attention with thorough outlier smoothing and per-thread int4 quantization. In *International Conference on Machine Learning (ICML)*, 2025. 3
- [70] Jinjin Zhang, Qiuyu Huang, Junjie Liu, Xiefan Guo, and Di Huang. Diffusion-4k: Ultra-high-resolution image synthesis with latent diffusion models. In *Proceedings of the IEEE/CVF Conference on Computer Vision and Pattern Recognition*, pages 23464–23473, 2025. 3
- [71] Jintao Zhang, Jia Wei, Pengle Zhang, Jun Zhu, and Jianfei Chen. Sageattention: Accurate 8-bit attention for plug-and-play inference acceleration. In *International Conference on Learning Representations (ICLR)*, 2025. 3

- [72] Jintao Zhang, Chendong Xiang, Haofeng Huang, Jia Wei, Haocheng Xi, Jun Zhu, and Jianfei Chen. Spargeattn: Accurate sparse attention accelerating any model inference. In *International Conference on Machine Learning (ICML)*, pages 76397–76413, 2025. 3
- [73] Kai Zhang, Jingyun Liang, Luc Van Gool, and Radu Timofte. Designing a practical degradation model for deep blind image super-resolution. In *Proceedings of the IEEE/CVF International Conference on Computer Vision*, pages 4791–4800, 2021. 1
- [74] Lvmin Zhang, Anyi Rao, and Maneesh Agrawala. Adding conditional control to text-to-image diffusion models. In *Proceedings of the IEEE/CVF International Conference on Computer Vision*, pages 3836–3847, 2023. 2
- [75] Michael Zhang, Kush Bhatia, Hermann Kumbong, and Christopher Ré. The hedgehog & the porcupine: Expressive linear attentions with softmax mimicry. In *International Conference on Learning Representations (ICLR)*, 2024. 3
- [76] Yuyao Zhang and Yu-Wing Tai. Scale-dit: Ultra-high-resolution image generation with hierarchical local attention. *arXiv preprint arXiv:2510.16325*, 2025. 3
- [77] Yuyao Zhang, Jinghao Li, and Yu-Wing Tai. Layercraft: Enhancing text-to-image generation with cot reasoning and layered object integration. In *Advances in Neural Information Processing Systems (NeurIPS)*, 2025. 1
- [78] Yuxuan Zhang, Yirui Yuan, Yiren Song, Haofan Wang, and Jiaming Liu. Easycontrol: Adding efficient and flexible control for diffusion transformer. In *Proceedings of the IEEE/CVF International Conference on Computer Vision*, pages 19513–19524, 2025. 6
- [79] Qingping Zheng, Yuanfan Guo, Jiankang Deng, Jianhua Han, Ying Li, Songcen Xu, and Hang Xu. Any-size-diffusion: Toward efficient text-driven synthesis for any-size hd images. In *Proceedings of the AAAI Conference on Artificial Intelligence*, pages 7571–7578, 2024. 3
- [80] Lianghui Zhu, Zilong Huang, Bencheng Liao, Jun Hao Liew, Hanshu Yan, Jiashi Feng, and Xinggang Wang. Dig: Scalable and efficient diffusion models with gated linear attention. In *Proceedings of the IEEE/CVF Conference on Computer Vision and Pattern Recognition*, pages 7664–7674, 2025. 3

HierEdit : Region-Aware Hierarchical Diffusion for Efficient High-Resolution Editing

Supplementary Material

8. Comparison with Upscaler Baselines.

Here we present a qualitative (Figure 8) example where the lady’s facial expression and posture totally changed. Both upscalers show artifacts (eyelash discontinuity and blurriness), while ours does not. We will add complete quantitative comparisons in the final version.

9. Example on Full Editing

Figure 9 further illustrates our ability to edit entire images, even though our focus is on local editing.

10. More Ablation Study

Ablation on Denoising Step Reduction. We further examine how aggressively denoising steps may be skipped while preserving output quality. Figure 10 presents results obtained by skipping $\{0, 10, 14, 18, 22, 24\}$ out of 28 total steps. Skipping 18 steps offers the best balance between visual quality and efficiency.

11. Implementation Details

11.1. Experimental Setup.

We adopt FLUX.1-dev [3] as our base model. The network is fine-tuned using LoRA with a rank of 16, trained for 10,000 steps with a batch size of 6 on six NVIDIA RTX A6000 Ada GPUs (48 GB each). All evaluations are performed on a NVIDIA RTX 6000 Ada Pro GPU (96 GB) server. For training, we employ the IPA300K dataset [77], which provides paired source and target images along with textual prompts and bounding-box annotations on 1024×1024 resolution. For the off the shelf low-resolution model selection, we choose either FLUX-Kontext.dev or OminiControl2. For kernel adaptation, we permute the token sequence to a ”window-first” way, so that the tokens within one local window will stick to each other in the sequence and we also adapt our code to Flash Sparse Attention [48], to skip the masked blocks for speeding up

11.2. Instructional Editing Benchmarks

We provide additional details regarding the quantitative comparisons in Table 1 in the main paper. We evaluate on I2EBench [33], ImgEdit [65], CompBench [22], and EmuEdit [47]. For the composite benchmarks (those measuring multiple subtasks), we average the scores of the local

editing tasks. The details for each benchmark are listed below.

I2EBench. The I2EBench benchmark, which encompasses 16 diverse image editing tasks spanning both low-level restoration and high-level semantic modifications. We evaluate on the the first category includes 9 low-level tasks: Deblurring, HazeRemoval, Lowlight, NoiseRemoval, RainRemoval, ShadowRemoval, SnowRemoval, WatermarkRemoval, and RegionAccuracy. We evaluate using the Structural Similarity Index (SSIM), comparing edited images against ground truth references.

CompBench. We evaluate on the local subset of the CompBench benchmark, which includes add, remove, and replace tasks. We report the average scores across those three tasks. For each task, we measure text-image alignment through the CLIP Score and structural similarity in background regions using SSIM.

EmuEdit. For the EmuEdit benchmark, we utilize the test split of the facebook/emu_edit.test.set dataset from HuggingFace, and report two metrics. The $CLIP_{dir}$ assesses directional alignment of the edit. The DINO score measures feature-level preservation.

ImgEdit. We evaluate our method on the ImgEdit benchmark using its basic suite, which consists of single-turn editing tasks. The primary evaluation relies on a GPT-4 judge. The judge model receives three inputs (the original image, the edited image, and the textual instruction) and produces three integer scores ranging from 1 to 5 for different aspects of the edit. These scores are averaged. We report these averages across a range of local editing tasks: add, adjust, compose, extract, remove, and replace.

12. More Examples

We present additional qualitative examples in Figures 12. The original images are upsampled using the BSRGAN super-resolution model [73]. For each example, the low-resolution edited result is displayed inside the black box located at the lower-left corner. We also include 4K (Figure 13) and 2K (Figure 14) editing results on synthetic data.

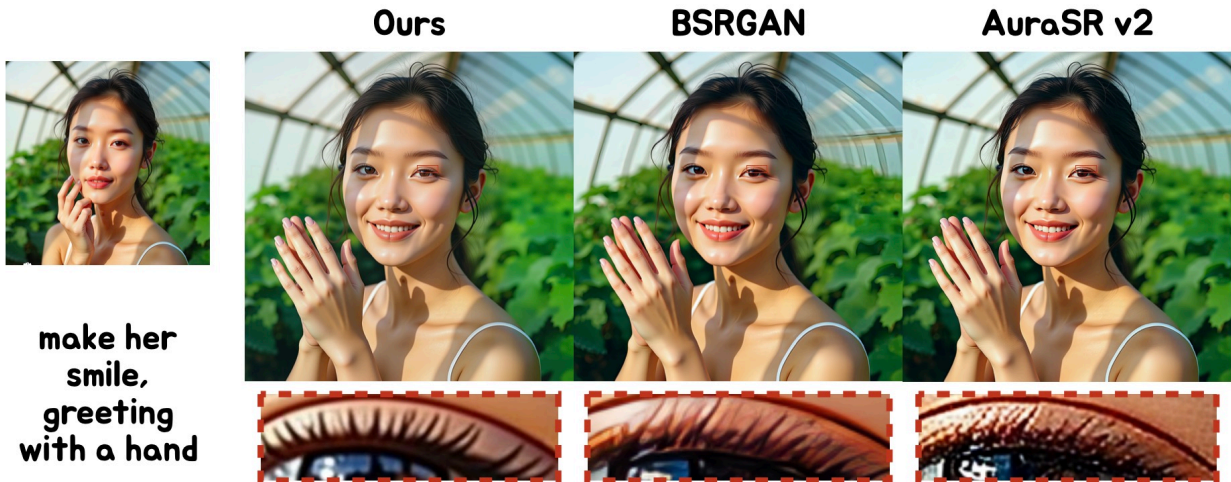


Figure 8. Comparison with low-resolution editing followed by upscaling.



Figure 9. Our model also supports full image editing by removing the mask although we focus on local editing.



Figure 10. Ablation on the number of timesteps skipped. Results shows 18 steps yields an optimal solution balancing the generation quality and speed. Numbers in red are PSNR values.

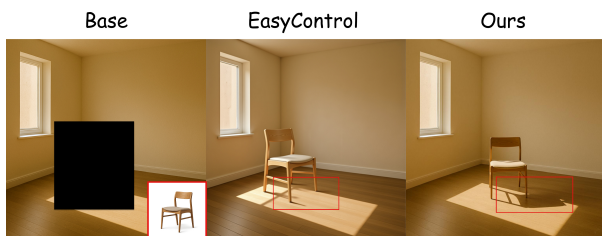


Figure 11. The inappropriate bounding box will lead to issues in correct shadowing or other artifacts, therefore we need to refine the bounding box.



make her smile,
greeting with a
hand



Can we have a
dog instead of
the cat looking
at the camera?



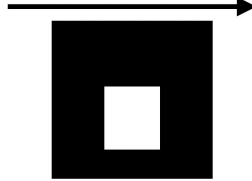
Add a flower
on the t-shirt
of the guy in
the middle with
dark jeans



Figure 12. More examples on 4K in-the-wild data.



Change the guy
in the mask to
snow white in
red dress



A boho chic lady
in a leather
trench
wandering

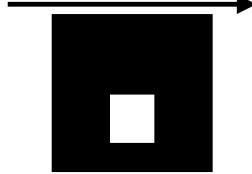


Figure 13. More examples on 4K synthetic data.



She is wearing a Chinese Qipao



Change it to blue bird



Change the moon to Saturn



An elf is jumping in the forest



Figure 14. More examples on 2K synthetic data.